JOURNAL OF FORENSIC SCIENCES

J Forensic Sci, March 2011, Vol. 56, No. 2
doi: 10.1111/j.1556-4029.2010.01643.x
Available online at: onlinelibrary.wiley.com

PAPER

PHYSICAL ANTHROPOLOGY

Andrew Wade,[1] *M.A.; Andrew Nelson,*[1] *Ph.D.; Greg Garvin,*[2] *M.D.; and David W. Holdsworth,*[3] *Ph.D.*

Preliminary Radiological Assessment of Age-related Change in the Trabecular Structure of the Human *Os Pubis**

ABSTRACT: This preliminary study examines correlations between age-at-death and changes in the trabecular architecture of the human *os pubis,* utilizing continuous, quantitative data from plain film radiography, computed tomography (CT), and micro-CT scans of 65 male innominates. Radiography provides nondestructive options for assessment, digital preservation, and presentation of human skeletal remains; important for forensic and culturally sensitive archaeological materials, which must remain unmodified for opposing experts, future researchers, or repatriation and reburial. Radiographic techniques permit analysis of remains that cannot be disarticulated (e.g., religious proscription, mummies), and trabecular measures provide data where traditional surface indicators are obscured or damaged. Potentially, robust predictive models derived herein achieve *R*-values of 0.522, 0.447, and 0.731, respectively. Further testing of these methods may validate these techniques as further lines of evidence in age estimation, with the potential to improve on the accuracy of traditional qualitative techniques by providing quantitative, continuous variables in predicting skeletal age-at-death.

KEYWORDS: forensic science, age estimation, plain film radiography, computed tomography, micro-CT, pubis, cancellous bone

One of the most common methods by which age-at-death is currently estimated from bone is based on macroscopic examination of the morphological changes occurring with age on the symphyseal surface of the pubis. Techniques pioneered by Todd (1), McKern and Stewart (2), and Brooks and Suchey (3) provide mean and age range estimates for each discrete phase of morphological change. Unfortunately, these qualitatively based estimates are non-continuous (broken into discrete or overlapping phases), present large error ranges, and are often represented by a mean value for the phase that is misleading because of asymmetric and non-Gaussian distributions within each phase (4). It is worth noting, however, that transition analysis may mitigate the last of these issues (4,5). Similar qualitative, stage-based methods exist for macroscopic evaluation of the morphology of the auricular surface of the ilia (6,7), the sternal rib ends (8,9), and closure of cranial sutures (10). Quantitative methods have been developed for the estimation of age from the microscopic histological assessment of osteonal bone remodeling in cortical (11,12) and cancellous bone (13), but require destructive sampling of the bone. Plain film radiographic techniques have been developed for age estimation from trabecular architecture in the femur, humerus, clavicle, and pubis (14–19), but are, like surface morphology techniques, qualitative and stage based. Computed tomography (CT) and micro-CT methods of age estimation are being increasingly explored, but many focus on imaging of external morphology (e.g., [20–25]).

The examination of the pubis using plain film radiography, CT, or micro-CT avoids destructive analysis of human remains while providing an opportunity to estimate age-at-death using continuous, objective, quantitative measures based on the remodeling of the cancellous bone that underlies the symphyseal surface. This study is inspired by findings by DeLaurier (26), who noted age-related structural change in pubic cancellous bone (Fig. 1). DeLaurier (26) found that,

> [c]hanges in the density and organization of the trabecular bone with advancing age parallel changes that occur on the cortical surface…After the age of 40 years, when the production of new bone ceases, the trabecular bone continues to degenerate…but individual fibers are not replaced, making the trabecular structure porous and weak. The existing trabeculae attempt to make up for this by becoming thicker… (p. 115).

This age-related degeneration of the pubic trabeculae was first noted in Todd's (16) radiographic study of the pubis, which found that changes in compacted structures, in the texture of the body of the pubis, and in the increasingly open mesh of trabeculae varied with age. By contrast, macroscopic methods evaluate structural changes in the less dynamic cortical bone. Given that cancellous bone experiences a nearly ninefold greater turnover rate compared with cortical bone (27), its morphology is more sensitive to metabolic conditions (including those related to aging) than the surface of cortical bone.

Radiographic imaging modalities provide an additional line of evidence for age estimation along with a nondestructive option for

[1]Department of Anthropology, University of Western Ontario, London, Ontario N6A 5C2, Canada.
[2]St. Joseph's Health Care, London, Ontario N6A 4V2, Canada.
[3]Robarts Research Institute, University of Western Ontario, London, Ontario N6A 5K8, Canada.
*Funding provided by the Ontario Graduate Scholarship of Andrew Wade and the Faculty Scholar Grant to Andrew Nelson.

Received 4 Nov. 2009; and in revised form 30 Jan. 2010; accepted 6 Feb. 2010.

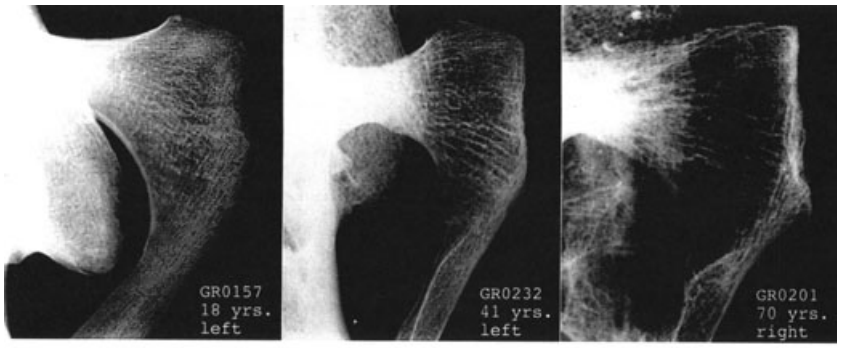

Fig. IV.3 Radiographs of non-diseased pubes from Grant sample. Note dense trabeculae with little orientation in the young specimen, decreasing density and stronger orientation of trabeculae in the middle-aged specimen, and low density, but retention of orientation of trabecualae in the older specimen.

FIG. 1—*Age-related trabecular changes noted by DeLaurier (26, p. 118).*

assessment, digital preservation, and electronic sharing of remains that are either incompatible with macroscopic techniques (i.e., damaged or fragmentary remains, wrapped mummies) or culturally sensitive and must remain articulated or completely unmodified.

Plain film radiography has a greater spatial resolution than CT (28,29) and is relatively inexpensive, widely available, and, with portable X-ray units, even accessible in the field for archaeological and forensic applications. CT scanners are largely restricted to clinical settings because of their size, sensitivity to harsh environments, and cost, but they offer a greater contrast resolution (distinguishing between materials' radiodensities) than plain film radiography (28,29). Although they are capable of better resolutions and are becoming more common and less costly, micro-CT scanners are more expensive and are further restricted in their availability and accessibility. Scanning times for micro-CT units are also considerably longer than they are for CT (minutes to hours for scan resolutions of 65 μm and better, as opposed to seconds for clinical CT). This trade-off, between resolution and cost, will influence decisions on the appropriateness of each modality for the situation at hand.

Ultimately, the goal of this line of inquiry was to identify useful relationships between bone microarchitecture and age-at-death; providing additional lines of evidence for age estimation using methods that access such relationships to fit a variety of needs and resources. Specifically, this study was intended to produce predictive models for age estimation based on accessible measures of trabecular density and architecture on each of the three radiographic imaging modalities and their correlation to the sample's ages at death. The utility of such models may then be tested on other samples of known age.

Materials and Methods

The skeletal remains used in this study were acquired from the Grant Collection, formed using unclaimed bodies as per the Anatomy Act of Ontario (30), and housed at the University of Toronto. At the time of their original receipt and dissection, in the 1920s through 1950s, the skeletal elements were inventoried, noting the age-at-death (later verified), sex, and cause of death of the individual. Individuals without a verified age-at-death were deemed to be unsuitable for this study. Individuals with no known cause of death listed could not be considered likely to be free of pathological conditions affecting bone and were also eliminated from the study.

The sample selected for this study consisted of a total of 65 male individuals, 10 per decade of life from 30 to 89 years ($n_1 = 60$) and as available from individuals in their 20s and 90s ($n_2 = 5$) (Fig. 2).

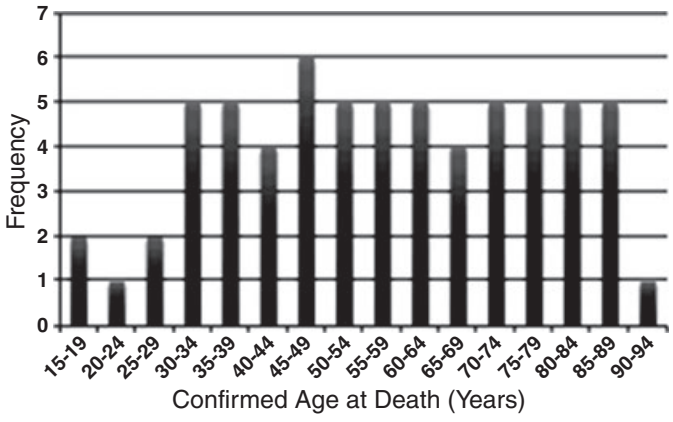

FIG. 2—*Graph of age distribution of sample.*

The specific region of interest (ROI) in this study extended from the pubic symphyseal surface to the midline of the obturator foramen parallel to the symphyseal surface. This region was imaged using plain film, CT, and micro-CT. Values of interest include (as resolutions and imaging modalities allow) bone and tissue volumes (TV); trabecular number (TbN), thickness (TbTh), and separation (TbSp); degree of anisotropy; and connectivity density (31).

Data Acquisition

Plain Film Radiography—The left pubis was X-rayed without an intensifying screen in the antero-posterior view for 2 min at 60 kV and 0.2 mA, using Kodak Ektavision 5 (EVG5) X-ray film (Kodak Canada, Toronto, Ontario, Canada) in a Faxitron model 43855A cabinet X-ray machine (Faxitron Xray Corporation, Wheeling, IL). The microfocus X-ray source used and the geometry of the pubis made magnification and distortion negligible factors. The developed films were then scanned at 600 dpi using a UMAX Powerlook 2100XL flatbed transmission scanner (Techville, Inc., Dallas, TX) and Magic Scan v.4 software (256 grayscale, mid-tone 2.0; Techville, Inc.).

Clinical CT—The innominates were scanned in a GE Lightspeed Volumetric Computed Tomography (VCT) 64 slice scanner (GE Healthcare, Chalfont St.Giles, Buckinghamshire, UK) at a within-scan resolution of 0.293 mm and a slice thickness of 0.625 mm (120 kV, 200 mA, axial). The ilium was supported to

keep the anterior aspect of the sample facing the CT bed and the medial aspect facing into the scanner gantry. The scan was then saved in Digital Imaging and Communications in Medicine (DICOM) format for processing in the GE Microview CT/micro-CT analysis software (http://microview.sourceforge.net/).

Micro-CT—The innominates were scanned at the Robarts Research Institute (University of Western Ontario) in a GE Locus Ultra micro-CT scanner, the highest resolution scanner capable of receiving a sample of this size, at a resolution of 150 μm (120 kV, 20.0 mA, 16.0 sec). A volumetric reconstruction (VFF [Volume File Format]) was created from the raw scanning data for processing in the GE Microview analysis software.

Data Processing

Plain Film Radiography—In the body of each pubis, a rectangular ROI was marked at right angles to the symphyseal surface (Fig. 3). One side was marked immediately behind the relatively dense symphyseal surface and extended to the obturator foramen without including cortical margins in the ROI. The scanned plain films, once marked with a scale and ROI in Photoshop CS3, were imported to the Image Pro Express 4.0 image analysis software (Media Cybernetics, Inc., Bethesda, MD). A line profile tool, measuring the grayscale pixel values along any given line, was used to measure the average intensity of the imaged trabecular structures along three lines in the ROI parallel to the symphyseal surface. These lines, running in a supero-inferior orientation, were located immediately inside the medial and lateral bounds of the ROI and at the midline of the ROI (Fig. 3). The line profile tool (thick horizontal setting) also measures mean values over a designated area and was used to measure values in the medial and lateral halves of the ROI. These linear and area profile means, along with their standard deviations and data for the height and width of the ROI, were recorded (Table 1).

In the plain film radiographs, linear trabecular density was defined as the number of intersections per millimeter and was derived from direct visual counts of trabeculae made using a high contrast image. The shadow and highlight were manually adjusted in GNU Image Manipulation Program (GIMP; TheGIMPTeam, http://www.gimp.org) 2.4.4 to a set of tonal levels that made visualization of the trabeculae easier. To mitigate intra-observer error, the whole number closest to the average of three consecutive direct visual counts was used to calculate linear trabecular density.

Clinical CT—The DICOM slices were imported into GE Microview analysis software, and reconstructions of the volumes were created for each individual. In each reconstruction, a cuboid volume of interest (VOI) was designated with one face immediately behind the symphyseal surface. The VOI was extended to include as large a volume of cancellous bone as possible without including cortical bone (Fig. 4).

Values of interest included bone surface (BS) and volume (BV); TV; TbN, TbTh, and TbSp; connectivity density (−Euler/Volume); and anisotropy by paired axes (a1/a2, a2/a3, and a1/a3) (Table 2). The ratio of BV to tissue (total) volume (BV/TV) of the VOI is a

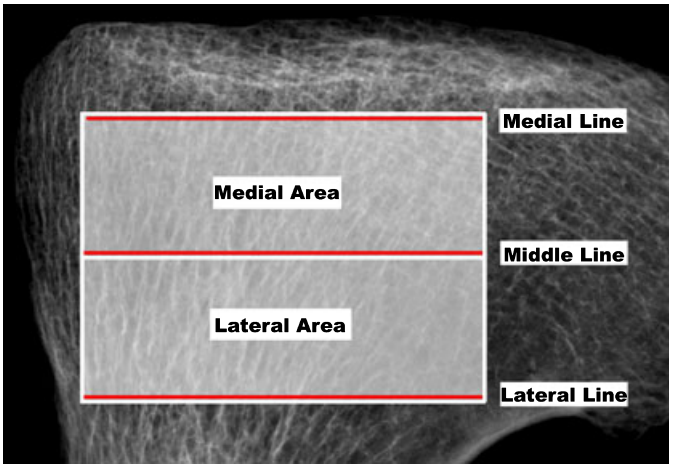

FIG. 3—*Lines and areas from which the plain film measures were drawn.*

TABLE 1—*Descriptive and correlative statistics (with age) for plain film variables.*

Plain Film Variables	Mean	Standard Deviation (SD)	*R* (w/age)	*p*
Medial Area Mean	43.51	9.404	−0.213	0.045
Medial Area SD	4.778	1.779	0.100	0.214
Lateral Area Mean	42.79	8.474	−0.204	0.051
Lateral Area SD	4.972	1.858	0.139	0.135
Total Area Mean	43.15	8.758	−0.213	0.044
Medial Linear Mean	51.38	10.71	−0.106	0.200
Medial Linear SD	8.779	1.909	0.105	0.204
Middle Linear Mean	40.81	8.658	−0.222	0.037
Middle Linear SD	8.116	1.985	0.234	0.030
Lateral Linear Mean	46.94	8.757	−0.162	0.098
Lateral Linear SD	7.949	1.816	0.138	0.137
Medial Linear Density	1.404	0.1924	−0.118	0.174
Middle Linear Density	1.369	0.1825	−0.006	0.480
Lateral Linear Density	1.240	0.1715	−0.017	0.445

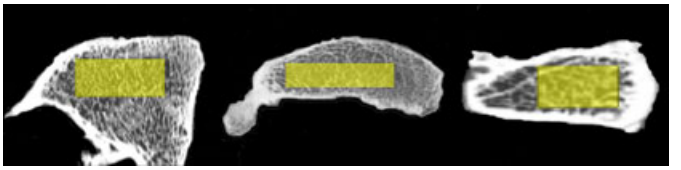

FIG. 4—*VOI defined in antero-posterior (left), medio-lateral, and supero-inferior (right) planes for a CT reconstruction.*

TABLE 2—*Descriptive and correlative statistics (with age) for CT variables.*

CT Variables	Mean	Std. Dev.	*R* (w/age)	*p*
−Euler/Volume	0.0327	0.0216	−0.096	0.224
BV/TV	0.334	0.0764	−0.061	0.315
BS/BV (*x*)	2.34	0.380	0.190	0.065
BS/BV (*y*)	1.89	0.216	−0.016	0.450
BS/BV (*z*)	2.00	0.277	−0.300	0.008
BS/BV (avg)	2.12	0.271	0.127	0.157
TbTh (*x*)	0.875	0.144	−0.184	0.071
TbTh (*y*)	1.07	0.120	−0.011	0.466
TbTh (*z*)	1.02	0.145	0.291	0.009
TbTh (avg)	0.975	0.122	−0.114	0.183
TbN (*x*)	0.384	0.0779	0.097	0.221
TbN (*y*)	0.311	0.0593	−0.065	0.303
TbN (*z*)	0.331	0.0754	−0.218	0.040
TbN (avg)	0.347	0.0646	0.028	0.412
TbSp (*x*)	1.85	0.629	−0.033	0.396
TbSp (*y*)	2.28	0.760	0.053	0.337
TbSp (*z*)	2.19	0.848	0.173	0.083
TbSp (xy avg)	2.07	0.683	0.014	0.455

BS, bone surface; BV, bone volume; CT, computed tomography; TbN, trabecular number; TbSp, trabecular separation; TbTh, trabecular thickness; TV, tissue volume.

measure of the overall bone density (31). A measure of the BS divided by the BV (BS/BV) is also provided by Microview (31). The average separation between trabecular edges (32) and thickness of trabeculae was also provided in terms of measurements along the *X* (supero-inferior), *Y* (antero-posterior), and *Z* (medio-lateral) axes, along with an average of the three axes. BS/BV is similarly presented, as is the TbN, a measure of the average linear trabecular density in each axial plane (32). Because the measures are averaged and the resolutions of both the CT and micro-CT scans are greater than one-half the width of a trabecula (33), the measures here, while considered to be variables of interest, are not considered to be precise measures of individual trabeculae (particularly on the *Z* axis in CT).

The connectivity of the trabeculae was measured by the Euler characteristic, which is related to the maximum number of trabeculae that can be severed in a trabecular structure without dividing the structure into two discrete parts (34). The connectivity density is equal to (1 − Euler#)/Volume and is expressed as the approximation −Euler#/Volume (35). The calculation requires the assumption of "trabeculae at the boundary of the VOI as connected to the adjacent trabecular network" (35, p. 1377) in order to avoid biasing *edge effects* seen in excised samples (36). This assumption is met here, as the VOI was completely surrounded by the remainder of the trabecular network.

Micro-CT—The VFF reconstructions were imported into Microview. In each reconstruction, a cuboid VOI was designated with one face immediately behind the symphyseal surface and the VOI was extended to include as large a volume of only cancellous bone as possible. Values of interest included, as for the CT analysis, bone and TVs; TbN, TbTh, and TbSp; and connectivity density (Table 3). Additionally, because the micro-CT scan's voxels are isotropic, a measure of anisotropy could be calculated (this property could not be assessed on the clinical CT data as the voxels were inherently anisotropic). Where a property of interest is unchanged by re-orientation, a structure is *isotropic* with respect to that property (34). The tendency of trabeculae to increasingly align in a particular direction was qualitatively observed in plain film radiographs and was considered an important variable to measure quantitatively in the micro-CT data.

TABLE 3—*Descriptive and correlative statistics (with age) for micro-CT variables.*

Micro-CT Variables	Mean	Standard Deviation	*R* (w/age)	*p*
−Euler/Volume	0.7310	0.5647	−0.502	0.000
BV/TV	0.2525	0.08006	−0.485	0.000
BS/BV (*x*)	6.893	0.7843	0.486	0.000
BS/BV (*y*)	6.515	0.5417	−0.174	0.083
BS/BV (*z*)	5.885	0.5772	−0.402	0.000
BS/BV (avg)	6.431	0.4707	0.039	0.380
TbTh (*x*)	0.2940	0.03477	−0.467	0.000
TbTh (*y*)	0.3091	0.02571	0.186	0.069
TbTh (*z*)	0.3444	0.03407	0.437	0.000
TbTh (avg)	0.3127	0.02330	−0.016	0.450
TbN (*x*)	0.8485	0.2103	−0.401	0.000
TbN (*y*)	0.8213	0.2616	−0.529	0.000
TbN (*z*)	0.7436	0.2448	−0.591	0.000
TbN (avg)	0.8045	0.2344	−0.523	0.000
TbSp (*x*)	0.9637	0.3555	0.411	0.000
TbSp (*y*)	1.047	0.4669	0.488	0.000
TbSp (*z*)	1.167	0.5378	0.517	0.000
TbSp (avg)	1.048	0.4392	0.481	0.000
a1/a3	1.391	0.2249	0.383	0.001
a1/a2	1.135	0.1060	0.251	0.022
a2/a3	1.223	0.1383	0.345	0.002

BS, bone surface; BV, bone volume; CT, computed tomography; TbN, trabecular number; TbSp, trabecular separation; TbTh, trabecular thickness; TV, tissue volume.

The anisotropy measure produced by the Microview software, Mean Intercept Length (MIL), is based on a count of interceptions between a linear grid and the trabecular structure. The mean distance between grid-bone intercepts is calculated from the measures in different orientations throughout 180° by dividing the total length of grid lines by the number of intersections with bone-air interfaces. This process is repeated in each of the three planes, and the results may be represented as an ellipsoid (34,37). The degree of anisotropy was then determined by comparing the maximum and minimum MIL measures of the major and minor axes of anisotropy, respectively (36).

Thresholding

Because the resolution of CT and micro-CT scans is finite, it is not possible to determine with complete certainty where one material ends, in this case bone, and the next begins, in this case air. This results in what is commonly referred to as a *partial volume effect*, in which "an object does not completely fill the thickness of a voxel (e.g., at the edge of a bone) resulting in imprecise boundary definition" (38, p. 185). The radiodensity value of the voxel is assigned an average of the radiodensities of the materials contained in the voxel (29). As such, it is necessary to provide the quantitative analysis software with a threshold value that distinguishes one material from another (39), in this case distinguishing bone from air. The determination of a suitable threshold value is important in quantitative analyses, as a difference in threshold of only 0.5% can result in BV fraction measures that differ by up to 5% (40). The most accurate method to determine a threshold is Archimedes' principle; measuring bone mass in water or another liquid of known density and again after drying to determine the ratio of BV to total volume (41,42). This method, however, is time-consuming (40) and not appropriate for use with samples from a scientific or archaeological collection because of the high potential for damage.

This study made use of the automated thresholding method present in the Microview analysis software used to reconstruct and measure trabecular structures. This widely applicable and highly stable automated method is based on the integrative method developed by Otsu (43). This method treats the grayscale histogram as a probability function on which discriminant functions are applied and maximized to determine the threshold that provides "the best separation of classes [in this case, bone voxels and air voxels] in grey levels" (43, p. 63).

Statistical Methodology

The variables were imported to SPSS 15.0 (IBM Corporation, Somers, NY), and a backward multiple regression (to prevent model overfitting) was performed using the variables in each modality to identify measures that were significant factors in the estimation of age. Because the number of variables was large, the adjusted R^2 value (adjusted multiple coefficient of determination) was consulted rather than the R^2 value (multiple coefficient of determination). This adjustment further prevents overfitting of the model (44, p. 597) by adjusting for the number of variables present.

It is possible to utilize multiple regression analysis here, because the variables are continuous measures rather than discretely scorable traits. Provided that the assumptions required for regression are met, multiple regression on continuous data "does not

inevitably lead to estimated ages that are necessarily inaccurate or imprecise" (45, p. 190). These assumptions were considered carefully, the variables tested for conformance, and in the case of the CT and micro-CT regressions adjustments were made (e.g., exclusion of z data from the TbSp average in the final CT model) where those assumptions would otherwise be violated.

Intra-observer error was assessed by processing scans using the established methodology and taking the appropriate measurements for a single different individual in each of the three modalities. This was repeated five times for the same individuals, trials separated by approximately 1 h each. Kruskal–Wallis and Friedman tests aimed at identifying differences between multiple samples/trials of identical individuals, for each modality showed no significant differences between trials (K–W results: plain film $p = 0.437$, CT $p = 0.448$, micro-CT $p = 0.448$; Friedman results: plain film $p = 0.837$, CT $p = 0.961$, micro-CT $p = 0.994$).

Inter-observer error was assessed by instructing two additional observers, with minimal experience with the analysis software, on the processing methodology and required measures. These observers were then tasked with processing a scan and taking the appropriate measurements for the same single individual, with the individual differing between the three modalities. Kruskal–Wallis and Friedman tests for each modality did not show significant differences between all three observers (K–W results: plain film $p = 0.448$, CT $p = 0.454$, micro-CT $p = 0.458$; Friedman results: plain film $p = 0.071$, CT $p = 0.946$, micro-CT $p = 0.717$). Under less conservative standards ($\alpha < 0.10$), inter-observer difference appears in the plain film measures, likely due to the sampling specificity of the linear mean values (Friedman $p = 0.03$). The linear trabecular densities, initially expected to be the most subjective, and the area mean values remained insignificantly different between observers (Friedman $p = 0.10$ and 0.11).

Results

Plain Film Radiography

The measures of trabecular density (Table 1) in the final plain film model (Table 4) account for a small, but statistically significant, amount of the total variability present ($R^2 = 0.272$, $p = 0.001$). The model includes all of the most medial area and linear measures, likely due to trabecular remodeling in response to or resulting in remodeling of the symphyseal surface. The Pearson correlation coefficients of each of these measures with age are negative (Medial Linear Mean $R = -0.106$; Medial Area Mean $R = -0.213$; Medial Linear Density $R = -0.118$), with only the Medial Area Mean demonstrating a significant relationship ($p = 0.045$) on its own, and together indicate decreased trabecular density with increasing age. The standard deviation of the Middle Linear Mean, however, increases with age, as indicated by the positive Pearson correlation coefficient with age of 0.234 ($p = 0.030$). This increased range of pixel values is likely due to the decreased presence of trabeculae with age, resulting in lower pixel values along the line, along with increased thickness of trabeculae with age, resulting in higher pixel values elsewhere along the line.

Computed Tomography

The final model for the CT modality (Table 4) also accounts for a significant amount of the variability present ($R^2 = 0.200$, $p = 0.001$) and includes two of the trabecular separation measures; TbSp(z) and TbSp(xy avg) (Table 2). According to the Pearson correlation coefficients of both measures with age ($R = 0.173$ and $R = 0.014$, respectively), the medio-lateral space and the average (x and y only) space between trabeculae increase with age, although not with statistically significant certainty. This may correspond with the decreased presence of trabeculae with increasing age, qualitatively observed in plain film radiographs. However, the medio-lateral component of trabecular separation [TbSp(z)] may be accentuated by the anisotropy of the voxels in CT scans, and the medio-lateral scanning orientation used in this investigation makes the medio-lateral measures less representative of reality because of the lower between-slice resolution relative to the within-slice resolution (this same voxel anisotropy made it impossible to properly assess anisotropy of trabecular architecture in the CT scans).

Micro-CT

The final model for the micro-CT imaging modality (Table 4) accounts for a significant amount of the variability present ($R^2 = 0.534$, $p = 0.000$) and includes the connectivity density measure [−Euler/Volume], two of the trabecular thickness measures [TbTh(y) and TbTh(z)], and a bone surface-to-volume measure [BS/BV(x)] (Table 3). According to the Pearson correlation coefficients with age of both thickness measures ($R = 0.186$, $p = 0.069$ and $R = 0.437$, $p = 0.000$, respectively), the antero-posterior and medio-lateral thicknesses of trabeculae are increasing with age, although only the latter relationship is conservatively statistically significant. These increases correspond with the compensatory thickening of trabeculae expected to result from the overall removal of trabecular structural elements. Also, as a result of this decreased trabecular presence, the connectivity density demonstrates a negative Pearson correlation coefficient with age ($R = -0.502$, $p = 0.000$); the presence of fewer structural elements results in fewer possible connections. The final measure, the supero-inferior bone surface-to-volume ratio, was found to increase with increasing age ($R = 0.486$, $p = 0.000$). This may be explained by the transition of trabeculae from more plate-like structures to more rod-like structures with age (46). As the

TABLE 4—*Final regression models developed in this study for each modality.*

Modality	Final Model	R	p	Standard Error of Regression	Mean % Prediction Error
Plain Film Radiography	Age = 82.950 − 2.187 Medial Area Mean + 1.163 Medial Linear Mean + 4.190 Middle Linear Standard Deviation − 17.512 Medial Linear Density	0.522	0.001	17.49	25.5
Computed Tomography	Age = 62.165 + 29.177 TbSp(z) − 33.399 TbSp(xy avg)	0.447	0.001	18.0	26.7
Micro-Computed Tomography	Age = −76.413 − 225.415 TbTh(y) − 6.535 Euler#/Volume + 10.200 BS/BV(x) + 399.347 TbTh(z)	0.731	0.000	13.99	19.9

BS, bone surface; BV, bone volume; TbSp, trabecular separation; TbTh, trabecular thickness.

TABLE 5—*Comparison of age estimation techniques by* R*-values.*

Technique	Collection	*N*	*R*
Plain Film Radiography (this study)	Grant	65	0.52
Computed Tomography (CT) (this study)	Grant	65	0.45
Micro-CT (this study)	Grant	65	0.73
Pubic Symphysis – Todd*	Grant	163	0.59
Pubic Symphysis – Suchey-Brooks*	Grant	163	0.62
Revised Auricular Surface (6)	Spitalfields	180	0.61
Fourth Sternal Rib-end†	U.S. cadaveric	93	0.85(η)
Osteon Counts – rib (52)	U.S cadaveric	154	0.77
Total Osteon Counts – fibula (12)	U.S. cadaveric	33	0.67
Cancellous Osteon Counts – iliac crest (13)	E.U. cadaveric	25	0.82
Symphyseal Surface CT – paired (23)	French cadaveric	74	0.86

*Beneteau (58).
†Iscan et al. (8).

trabeculae become increasingly rod-like, their surface area is increased relative to their volume (47), resulting in a higher bone surface-to-volume ratio.

Discussion

The techniques developed in this study address two major problems present in many existing age estimation methods; the subjectivity of many qualitative methods and the discontinuous nature of stage-based assessment of surface features of bone. These techniques, for use in conjunction with other quantitative and qualitative techniques, offer a further line of evidence in age estimation, particularly where options for assessment are limited to examination of the pelvis or to nondestructive methods. While the proposed techniques do not appear to improve upon the precision attained by existing methods (Table 5), the continuous nature of age estimates made using these plain film, CT, and micro-CT techniques makes them potentially more accurate, even if not more precise, methods of estimating age-at-death. Rather than producing a mean age for one or two of five to 10 discrete stages with confidence intervals that overlap considerably between stages, the techniques described here produced continuous age estimates with 95% confidence intervals of between ±28 and ±35 years. In this study, the regression equations produced standard errors of regression and mean percent prediction errors ([(observed − predicted)/predicted] × 100%) of 17.49% and 25.5% for the plain film technique, 18.0% and 26.7% for the CT technique, and 13.99% and 19.9% for the micro-CT technique (Table 4). Both error measures are recommended as indicators of predictive power that are as important, or more so, than the correlation coefficient alone (48).

Qualitatively, the plain film radiographs of the pubis demonstrate an increasingly open mesh of trabeculae with age, as noted by Todd (16). The trabeculae appear thicker and less numerous with age and, as noted by DeLaurier (26), appear to be increasingly oriented medio-laterally. Quantitatively, the results in all three modalities are in agreement with these findings. The mean pixel values and the trabecular density measure in the plain film radiographs decrease with increasing age, indicating decreased overall density of trabeculae. The increased standard deviation demonstrates the greater range of values resulting from the presence of a decreased number of thicker trabecula. The possibly increasing TbSp values in the CT scans; the increasing TbTh in the micro-CT scans; and the increasing bone surface-to-volume ratio (micro-CT) also agree with this trend. Finally, the significantly decreasing connectivity of trabeculae in the micro-CT results follows as a result of this rarification of trabeculae with increasing age.

In accordance with the best practices in age estimation (see [49–55]), this study has made use of a reference sample with a uniform age distribution, to diminish target-reference bias, and that is representative of as much of the adult human age range as possible (Fig. 2). However, it should be noted that at this stage the sample is male specific for the sake of experimental simplicity and the techniques may not be equally applicable to females, owing to pelvic and cancellous bone changes related to parity and menopause. The quantitative age indicators (Tables 1–3) are unidirectional, continuous, and, most importantly, repeatably observable. Many individual measures demonstrated strong correlations with age, and the predictive models developed from them account for significant amounts of the variability present.

At this stage, the techniques developed in this study appear to compare favorably with existing methods of age estimation from skeletal remains in terms of explaining variability related to age, indicating that they may present useful additional or alternative lives of evidence (Table 5). The plain film and CT techniques approximate the correlation coefficients (*R*) achieved by the Todd (1) and Suchey-Brooks (3) pubic symphysis age estimation techniques. The micro-CT technique approximates the *R*-values of the destructive cancellous osteon count method (13) and the CT analysis of the surface morphology of paired pubes (23). The micro-CT technique even fairs favorably against precise thin section cortical osteon counts, in terms of this study's standard error of the regression (13.99) and that of the osteonal method of Cho et al. (12.22) (52). Age and sex biases and population variation comparisons (cf. [52–56]), however, cannot be made without further testing of these techniques on more and larger samples.

Large sample validation studies are required to better understand the accuracy of these techniques and the effects of factors, such as sex, ancestry, activity, health, and climate. Both left and right pubes should be incorporated into further investigations, both as a source of confirmation of estimated skeletal age in light of possible asymmetry (cf. [57]) and as a check against pathological conditions that affect pelvic trabeculae and may do so asymmetrically (e.g., Paget's disease of bone). The lack of anisotropy measures in the plain film radiographic modality, where increased medio-lateral orientation of trabeculae is qualitatively apparent, should be addressed in future studies. Investigation into alternative and multiple CT scanning orientations would also be advisable because of the difference between the in-plane resolution and the slice thickness. The anisotropy that this difference creates in CT voxels resulted in medio-lateral measures of trabeculae that were not representative of their true dimensions, and in a lack of usable CT anisotropy measures. CT and micro-CT techniques, when applied to dry bone remains, require optimized scanning protocols to account for the absence or desiccation of soft tissue. Scans at greater resolutions, meanwhile, will require improvements in micro-CT technology as available scanners do not allow whole innominates to be scanned at resolutions higher than those used here. Further testing with larger samples is needed before more can be said about the models' reliability and robusticity. Synthetic approaches, including analysis of concurrent changes in the trabecular architecture of the femoral neck, lumbar vertebrae, and pelvis, could also serve to distinguish the trabecular changes resulting from biomechanical stresses from those resulting from other factors such as age.

Conclusion

Qualitative stage-based estimates are noncontinuous, often represented by a misleading phase mean, and present large error ranges. Unlike traditional stage-scored traits, the proposed quantitative age

indicators are unidirectional, continuous, and repeatable, resulting in models that have the potential to produce age estimates more accurately than stage-based surface morphology techniques. The proposed techniques do not appear, however, to improve upon the precision attained by existing methods as the models produce 95% prediction intervals of between ±28 and ±35 years; decreasing from plain film and CT to micro-CT. Unfortunately, in the absence of greater refinement, this provides an estimation that is little better than assignment to young, middle age, or old age categories.

These radiographic techniques provide an additional, nondestructive line of evidence to assess age categories, of particular value where traditional macroscopic indicators are not available. The plain film technique relies on the most easily accessible resources and provides an estimation of age-at-death even when the symphyseal face is damaged and traditional macroscopic assessment from the pubic symphysis is not possible. The clinical CT technique, while not an improvement on accuracy or precision over plain film radiography, remains an important option for pelves that cannot be disarticulated or are inaccessible, such as those in wrapped mummies, burn cases, or fragmented mass disaster remains. When resources allow, the micro-CT technique produces the most accurate and precise results of the three modalities and, as in the case of plain film radiography, is a valuable tool when the symphyseal face is damaged and other indicators are inaccessible.

Acknowledgments

Scanning time was donated by St. Joseph's Healthcare, London (CT) and by the Robarts Research Institute (micro-CT). We thank Karen Betteridge and Rosemary Miller at St. Joseph's and Joseph Umoh at Robarts for technical assistance. Skeletal samples were provided by the Grant Skeletal Collection and the Dakhleh Oasis Project (pilot study). We thank, also, the article's anonymous reviewers for their valuable comments and critiques of the manuscript and Alyson Jaagumagi and Jennifer Morgan for their contribution to the inter-observer error testing.

References

1. Todd TW. Age changes in the pubic bones, I: the white male pubis. Am J Phys Anthropol 1920;3:285–334.
2. McKern TW, Stewart TD. Skeletal age changes in young American males. Natick, MA: Quartermaster Research and Development Command Technical Report, 1957.
3. Brooks ST, Suchey JM. Skeletal age determination based on the os pubis: a comparison of the Ascadi-Nemeskeri and Suchey-Brooks methods. J Hum Evol 1990;5(3):227–38.
4. Konigsberg LW, Herrmann NP, Wescott DJ, Kimmerle EH. Estimation and evidence in forensic anthropology: age-at-death. J Forensic Sci 2008;53(3):541–57.
5. Boldsen JL, Milner GR, Konigsberg LW, Wood JM. Transition analysis: a new method for estimating age from skeletons. In: Hoppa RD, Vaupel JW, editors. Paleodemography: age distributions from skeletal samples. New York, NY: Cambridge University Press, 2002;73–106.
6. Buckberry JL, Chamberlain AT. Age estimation from the auricular surface of the ilium: a revised method. Am J Phys Anthropol 2002;119(3): 231–9.
7. Lovejoy CO, Meindl RS, Pryzbeck TR, Mensforth RP. Chronological metamorphosis of the auricular surface of the ilium: a new method for determination of adult skeletal age at death. Am J Phys Anthropol 1985; 68:15–28.
8. Iscan MY, Loth SR. Determination of age from the sternal rib in White males: a test of the Phase Method. J Forensic Sci 1984;31:122–32.
9. Iscan MY, Loth SR. Determination of age from the sternal rib in White females: a test of the Phase Method. J Forensic Sci 1985;31:990–9.
10. Meindl RS, Lovejoy CO. Ectocranial suture closure: a revised method for the determination of skeletal age at death based on the lateral-anterior sutures. Am J Phys Anthropol 1985;65:147–56.
11. Kerley ER. The microscopic determination of age in human bone. Am J Phys Anthropol 1965;23:149–63.
12. Stout SD, Stanley SC. Percent osteonal bone versus osteon counts: the variable of choice for estimating age at death. Am J Phys Anthropol 1991;86(4):515–9.
13. Boel LW, Boldsen JL, Melsen F. Double lamellae in trabecular osteons: towards a new method for age estimation by bone microscopy. Homo 2007;58:269–77.
14. Macchiarelli R, Bonioli L. Linear densitometry and digital image processing of proximal femur radiographs: implications for archaeological and forensic anthropology. Am J Phys Anthropol 1994;93:109–22.
15. Szilvassy J, Kritscher H. Estimation of chronological age in man based on the spongy structure of long bones. Anthropol Anz 1990;48:289–98.
16. Todd TW. Age changes in the pubic bone: VIII. Roentgenographic differentiation. Am J Phys Anthropol 1930;14(2):255–71.
17. Walker R, Lovejoy CO. Radiographic changes in the clavicle and proximal femur and their use in the determination of skeletal age at death. Am J Phys Anthropol 1985;68:67–78.
18. Schranz D. Age determination from the internal structure of the humerus. Am J Phys Anthropol 1970;17:263–70.
19. Acsadi G, Nemeskeri J. History of human life span and mortality. Budapest: Akademiai Kiado, 1970.
20. Barrier P, Dedouit F, Braga J, Joffre F, Rouge D, Rousseau H, et al. Age at death estimation using multislice computed tomography reconstructions of the posterior pelvis. J Forensic Sci 2009;54(4):773–8.
21. Cooper DML, Thomas CDL, Clement JG, Turinsky AL, Sensen CW, Hallgrimsson B. Age-dependent change in the 3D structure of cortical porosity at the human femoral midshaft. Bone 2007;40(4):957–65.
22. Ferrant O, Rouge-Maillart C, Guittet L, Papin F, Clin B, Fau G, et al. Age at death estimation of adult males using coxal bone and CT scan: a preliminary study. Forensic Sci Int 2009;186:14–21.
23. Pasquier E, Pernot LSM, Burdin V, Mounayer C, Le Rest C, Colin D, et al. Determination of age at death: assessment of an algorithm of age prediction using numerical three-dimensional CT data from pubic bones. Am J Phys Anthropol 1999;108:261–8.
24. Telmon N, Gaston A, Chemla P, Blanc A, Joffre F, Rouge D. Application of the Suchey-Brooks method to three-dimensional imaging of the pubic symphysis. J Forensic Sci 2005;50(3):261–8.
25. Tocheri MW, Razdan A, Dupras T, Liu D, Bae M. Quantitative analyses of human pubic symphyseal morphology using three dimensional data: the potential utility for aging adult human skeletons. Proceedings of the 54th Annual Meeting of the American Academy of Forensic Sciences; 2002 Feb 10–16; Atlanta, GA. Colorado Springs, CO: American Academy of Forensic Sciences, 2002.
26. DeLaurier A. The effects of habitual biochemical stress, trauma and pathology on the development and age-related degeneration of the male pubic symphysis [MA thesis]. London (Ontario): University of Western Ontario, 1998.
27. Ruegsegger P, Durand EP, Dambacher MA. Differential effects of aging and disease on trabecular and compact bone density of the radius. Bone 1991;12(2):99–105.
28. Bushberg JT, Seibert JA, Leidholdt EM Jr, Boone JM. The essential physics of medical imaging, 2nd edn. New York, NY: Lippincott Williams & Wilkins, 2002.
29. Spoor CF, Jeffery N, Zonneveld FW. Imaging skeletal growth and evolution. In: O'Higgins P, Cohn MJ, editors. Development, growth, and evolution: implications for the study of the hominid skeleton. San Diego, CA: Academic Press, 2000;123–61.
30. Bedford ME, Russell KF, Lovejoy CO, Meindl RS, Simpson SW, Stuart-Macadam PL. Test of the multifactorial aging method using skeletons with known ages-at-death from the Grant collection. Am J Phys Anthropol 1993;91(3):287–97.
31. Borah B, Gross GJ, Dufresne TE, Smith TS, Cockman MD, Chmielewski PA, et al. Three-dimensional microimaging (MRmicroI and microCT), finite element modelling, and rapid prototyping provide unique insights into bone architecture in osteoporosis. Anat Rec B New Anat 2001; 265:101–10.
32. Parfitt AM, Brezner MK, Glorieux FH, Kanis JA, Malluche H, Meunier PJ, et al. Bone histomorphometry: standardization of nomenclature, symbols, and units. Report of the ASBMR Histomorphometry Nomenclature Committee. J Bone Miner Res 1987;2:595–610.
33. Nyquist H. Certain topics in telegraph transmission theory. Proc IEEE 2002;90(2):280–305 (originally published 1928).
34. Odgaard A. Three-dimensional methods for quantification of cancellous bone architecture. Bone 1997;20(4):315–28.

35. Kim D, Christopherson GT, Dong XN, Fyhrie DP, Yeni YN. The effect of microcomputed tomography scanning and reconstruction voxel size on the accuracy of stereological measurements in human cancellous bone. Bone 2004;35:1375–82.
36. Odgaard A, Gundersen HJG. Quantification of connectivity in cancellous bone, with special emphasis on 3-D reconstructions. Bone 1993;14:173–82.
37. de Oliveira LF, Lopes RT, de Jesus EFO, Braz D. 3D X-ray tomography to evaluate volumetric objects. Nucl Instrum Methods Phys Res A 2003;505:573–6.
38. Ruff CB, Leo FP. Use of computed tomography in skeletal structure research. Yearb Phys Anthropol 1986;29:181–96.
39. Coleman MN, Colbert MW. Technical note: CT thresholding protocols for taking measurements on three-dimensional models. Am J Phys Anthropol 2007;133:723–5.
40. Hara T, Tanck E, Homminga J, Huiskes R. The influence of microcomputed tomography threshold variations on the assessment of structural and mechanical trabecular bone properties. Bone 2002;31(1):107–9.
41. Ding M, Odgaard A, Hvid I. Accuracy of cancellous bone volume fraction measured by micro-CT scanning. J Biomech 1999;32(3):323–6.
42. Sharp DJ, Tanner KE, Bonfield W. Measurement of the density of trabecular bone. J Biomech 1990;22(8):853–7.
43. Otsu N. A threshold selection method from gray-level histograms. IEEE Trans Syst Man Cybern 1979;SMC-9(1):62–6.
44. McClave JT, Sincich T. Statistics, 9th edn. Upper Saddle River, NJ: Prentice Hall, 2003.
45. Lucy D, Aykroyd RG, Pollard AM, Solheim T. A Bayesian approach to adult human age estimation from dental observations by Johanson's age changes. J Forensic Sci 1996;41(2):189–94.
46. van Ruijven LJ, Giesen EBW, Mulder L, Farella M, van Eijden TMGJ. The effect of bone loss on rod-like and plate-like trabeculae in the cancellous bone of the mandibular condyle. Bone 2005;36(6):1078–85.
47. Day JS, Ding M, Odgaard A, Sumner DR, Hvid I, Weinans H. Parallel plate model for trabecular bone exhibits fraction-dependent bias. Bone 2000;27(5):715–20.
48. Smith RJ. Allometric scaling in comparative biology: problems of concept and method. Am J Physiol Regul Integr Comp Physiol 1984;246:152–60.
49. Bocquet-Appel JP, Masset C. Farewell to paleodemography. J Hum Evol 1982;12:321–33.
50. Buikstra JE, Konigsberg LW. Paleodemography: critiques and controversies. Am Anthropol 1985;87(2):316–33.
51. Hoppa RD, Vaupel JW. Paleodemography: age distributions from skeletal samples. Cambridge, UK: Cambridge University Press, 2002.
52. Cho H, Stout SD, Madsen RW, Streeter MA. Population-specific histological age-estimating method: a model for known African-American and European-American skeletal remains. J Forensic Sci 2002;47(1):12–8.
53. Berg GE. Pubic bone age estimation in adult women. J Forensic Sci 2008; 53(3):569–77.
54. Hens SM, Rastelli E, Belcastro G. Age estimation from the human os coxa: a test on a documented Italian collection. J Forensic Sci 2008; 53(5):1040–3.
55. Hoppa RD. Population variation in osteological aging criteria: an example from the pubic symphysis. Am J Phys Anthropol 2000; 111(2):185–91.
56. Kimmerle EH, Konigsburg LW, Jantz RL, Baraybar JP. Analysis of age-at-death estimation through the use of pubic symphyseal data. J Forensic Sci 2008;53(3):558–68.
57. Overbury RS, Cabo LL, Dirkmaat DC, Symes SA. Asymmetry of the os pubis: implications for the Suchey-Brooks method. Am J Phys Anthropol 2009;139:261–8.
58. Beneteau MB. The Grant collection: A test of the performance of the Todd technique and the Suchey-Brooks technique as indicators of age at death. Unpublished manuscript on file, Grant collection, University of Toronto, n.d.

Additional information and reprint requests:
Andrew Wade, M.A.
Anthropology Department
University of Western Ontario
London
Ontario N6A 5C2
Canada
E-mail: awade4@uwo.ca